KSME

Springer

Journal of Mechanical Science and Technology 34 (9) 2020

Original Article
DOI 10.1007/s12206-020-0840-x

Keywords:
· Biomedical devices
· Dynamics property
· High-speed photography
· Jet power
· Micro-jet technology
· Needle-free injection

Correspondence to:
Yong Kang
kangyong@whu.edu.cn

Citation:
Zeng, D., Wu, N., Qian, L., Shi, H., Kang, Y. (2020). Experimental investigation on penetration performance of larger volume needle-free injection device. Journal of Mechanical Science and Technology 34 (9) (2020) 3897~3909.
http://doi.org/10.1007/s12206-020-0840-x

Received November 20th, 2019
Revised February 17th, 2020
Accepted June 24th, 2020

† Recommended by Editor Sehyun Shin

Experimental investigation on penetration performance of larger volume needle-free injection device

Dongping Zeng[1,2,3], Ni Wu[1,2,3], Lei Qian[1,2,3], Hanqing Shi[1,2,3] and Yong Kang[1,2,3]

[1]School of Power and Mechanical Engineering, Wuhan University, Wuhan 430072, China, [2]Hubei Key Laboratory of Accoutrement Technique in Fluid Machinery and Power Engineering, Wuhan University, Wuhan 430072, China, [3]Hubei Key Laboratory of Waterjet Theory and New Technology, Wuhan University, Wuhan 430072, China

Abstract The injection performance of a small volume of needle-free injection (up to 0.3 mL) has proven to be controllable and satisfactory in transdermal drug delivery. However, no comprehensive research on the behavior of larger volume injections with different requirements for clinical applications exists. This study aims to present the penetration characteristics of larger volume injections, including dynamic properties, dispersion pattern, and percent delivery. The researchers conduct impact and injection experiments with injection volumes from 0.1-1.0 mL, driving pressures of 0.5-1.75 MPa, and orifice diameters of 0.17-0.5 mm. This study uses high-speed photography and impact experiments to capture the dynamic properties of the liquid jet. The researchers observe the dispersion patterns of liquid penetration into the gels in the gel injection experiments and investigate the percentages of liquid delivered to the skin tissues in porcine tissues injection experiments. Moreover, this study uses the response surface methodology (RSM) to analyze the interactive effect between various injection parameters on the injection performance. Results describe the differences in penetration performance between larger volume injections and small volume injections, and the critical volume of the mentioned injections is approximately 0.6 mL.

1. Introduction

The advent of the needle-free injection system for transdermal drug delivery has attracted attention in recent decades. Several macromolecules, including vaccines and growth hormones were administrated by the needle-free injectors [1-3]. The advantages of this technique include elimination of needle phobia, operability of self-administration, and fast drug delivery. This device enables the liquid drug to penetrate the skin by pressurizing it within the ampoule and propelling it through a small nozzle. Thereby, the needle-free injector was widely used to deliver drugs intradermally, subcutaneously, and intramuscularly using a high-speed stream of liquid drug without needles [4-6]. Although the needle-free injection has distinct advantages over conventional needle injection, it still shows low acceptance from patients in the clinic applications due to complaints about painful bruising and bleeding experiences after injection [7, 8].

A major concern in these injectors now is to continue to improve the controllability of the jet speed and injection depth for larger volume injection. Different types of needle-free injectors, including Lorentz-force and piezoelectric actuators can control the jet speed during small volume drug delivery [9-11]. These devices driven by piezoelectric or laser precisely could deliver the liquid drugs to the target tissue for the 0.01 mL volume injection [12, 13]. The injectors actuated by electric motors have demonstrated precise delivery of up to 0.3 mL [14, 15]. Recently, an urgent need persists to control the injection performance of needle-free injections with injection volumes exceeding 0.3 mL, because several common injections, such as vaccines, monoclonal antibodies, and hormones, are operated with 1.0 mL or greater doses in clinic practice [16, 17]. Many researchers have proposed that the electric motors and mechanical amplifiers

are worth exploring in the larger volume injection [18, 19]. In addition, some of them pointed out that understanding the requirements of the larger volume injection is the key to addressing the controllability in clinic application [20-22]. They believe that the compound ampoule producing two phases jet speed is an efficient way to control the injection performance in larger volume injection.

Meanwhile, penetration of fluid into tissue is related to many variables, including the orifice diameter, driving pressure, jet velocity and viscosity, and material stiffness. The peak and average stagnation pressures of the jet were directly influenced by the driving pressure and nozzle diameter [23]. Previous studies indicated that the driving pressure significantly affected the depth of penetration and the volume and density mainly varied the dispersion pattern [24, 25]. Another research attempted to obtain an optimal design with various parameters of this biomedical engineering device by using CFD models [26, 27]. In addition, a distinct difference exists in injection depth under various driving pressures for materials of low density and viscosity [28-30]. Although the mentioned studies have shown some requirements and characteristics for the successful delivery in the larger volume injections, no established criteria to distinguish between larger and small volume injections exists. Furthermore, research involving the interactive effects of injection parameters on the penetration performance for larger volume injections remain limited. Therefore, this study must gain a comprehensive understanding of the various characteristics of the larger volume injections.

This study focused on the jet dynamic properties and penetration characteristics of the larger volume needle-free injection. The researchers used a high-speed photography to visualize the behavior of jets penetrating the gels and the early jet dynamics features of needle-free injections with various injection volumes. Then, the researchers conducted the impact experiments to confirm the results of high-speed photography experiments, revealing the differences between larger volume injections and small volume injections in terms of pressure characteristics. In addition, this study quantitatively analyzed the interactive effects between various injection parameters on the penetration performance in injection through the response surface methodology (RSM). The researchers implemented the impact experiments and injection experiments and varied the injection volume between 0.1 and 1.0 mL, the driving pressure was between 0.5 and 1.75 MPa, and the orifice diameter was between 0.17 and 0.5 mm. Resultantly, the interactive effects between different injection parameters on the injection depth, width of dispersion region, and percent delivery were exhibited through the gel injection experiments and porcine tissue injection experiments. The result gained from these experiments would serve as guidelines for distinguishing the larger volume injection from the small volume injection and a reference for achieving controllability of larger volume injections under certain requirements.

Table 1. Air-powered needle-free injector parameters.

Driving pressure	3-15 Bar
Nozzle diameter	100-500 μm
Injection volume	0-1.0 mL
Piston diameter	33.8 mm
Piston distance	42-56 mm
Plunger diameter	7.9 mm
Plunger distance	5.9-19.9 mm

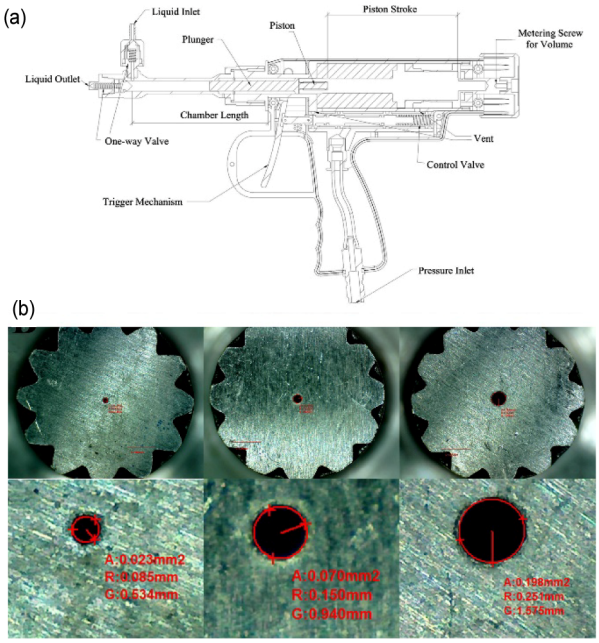

Fig. 1. (a) The schematic diagram of the air-powered needle-free injector and different nozzles; (b) nozzles with orifice diameter of 0.17 mm, 0.30 mm, and 0.50 mm.

2. Materials and method

2.1 Experimental setup

This study used a commercially available air-powered needle-free injector ([Patent No: ZL 201520432727.7] Sanxin Medical Technology Co., Ltd., Jiangxi Province, China) to administer 0.3-1.0 ml injections at 0.5-1.75 MPa driving pressures (Table 1). In this study, the researchers powered the injector by pressurized carbon dioxide gas and multiple injections could be performed through this device (Fig. 1(a)). The working process of the device includes three stages: initial state, gas enters the chamber from the pressure inlet and vent to push the impact piston and pull the plunger back to the starting position; injection process, once the trigger is pulled, the gas flows through the vent under the action of the control valve, pushing the impact piston and then hitting the plunger, thereby the liquid in the chamber is pushed out by the plunger through the nozzle; return to initial state, when the trigger is released and returned to the original position, the remaining gas in the cavity pushes

the impact piston backwards under the action of the control valve. The impact piston and the plunger return to the original position. The researchers used a metering screw to control the strokes of the piston and plunger. The researchers used the screw in conjunction with the check valves at the liquid inlet and outlet to adjust the injection volume. The researchers fully filled the chamber at each injection, thus the influence of fill ratio on the injection performance presented in previous research could be ignored [31]. Moreover, the nozzles with three sizes (0.17 mm, 0.30 mm, and 0.50 mm) of the injection presented in Fig. 1(b) were manufactured from stainless steel with a precision of 0.00326 mm, which is less than 1.91 % of all orifice diameter sizes.

2.2 Materials

To obtain a real time analysis of jet mechanics, the 10 % w/t ballistic gelatin has been used to mimic the muscle tissue due to its transparency and the material characteristics [24, 32]. In addition, the elastic modulus of 10 % gelatin (0.815 MPa) is close to it of muscular tissue (0.827 MPa). This gelatin was mixed by 10 % per weight gelatin powder (250 bloom, Sigma Aldrich, USA) and 90 % per weight distilled water under different conditions. The porcine tissue was typically used in the needle-free injection studies to simulate the human dermal tissue owing to comparability of the thickness of the stratum corneum, the stiffness of tissues, and analogous jet speed in ex-vivo human and porcine tissue [9, 33]. This study obtained post-mortem tissues through the Experimental Animal Center of the Wuhan University (Wuhan, China) using procedures approved by Hubei Provincial Experimental Animal Quality Inspection Station for scientific research (Permission license NO: SCXK2018-0187). This study harvested the tissues from the abdomen of pigs (approximately 4.5 months) immediately after euthanasia and included muscle and partial skin tissue and subcutis. The researchers trimmed, immediately vacuum sealed, and stored the tissue at −80 °C. Prior to injection, the researchers thawed each sample at 22 °C and equilibrated to room temperature.

2.3 Methods

To obtain the impact pressure of the injector during the entire injection process, this study established a test platform dedicated to presenting and recording the pressure behavior over a short period which is similar to the previous research [34, 35]. This platform comprises a dynamic pressure sensor (M5156-000002-030BG), an HBM data acquisition system (Quantum MX840B-8), and an integrated device with embedded Java programming language. The impact pressure could be calculated by the integrated device with embedded Java programming language in accordance with momentum theorem and Bernoulli equation from the impact force obtained by the test. The researchers performed three injections at each data point in the injection experiments. The researchers used the average value of the three injected experimental data to analyze the experimental phenomenon.

This study measured the injection depth and the width of the dispersion region in the gel injection experiments and obtained the delivery percent in the porcine tissue injection experiments. The injection depth was the total depth of dispersion; the injection width was the width of dispersion region. Moreover, the researchers used a high-speed video camera (Vision Research, Phantom V2012) to record the injection process for free jet injection in air and gels injection. The matching lens was provided by Nikon ED (AF Micro Nikkor 200 mm 1:4 D) at frame rates of 43000 fps with exposure times of 22 μs and an arrangement of halogen LED lamps were configured for this experiment. The effective resolution is 2000 * 3595 pixels under this configuration. The researchers calibrated the high-speed camera before test shooting. During the shooting of the experiment, the high-speed camera started to work before the injection behavior so that the entire injection process can be captured. After the shoot, this study used the Phantom Camera Control (version 2.0) to process the captured video. The point at which the droplet appeared at the nozzle was the beginning of the injection, and the jet exited the nozzle completely as the end point.

In addition, the view angle between the captured scope and the camera adds an error, e_s, into the length calculation on the basis of the images (Eqs. (1) and (2)).

$$e_s = 1 - \cos^4 \theta_s \tag{1}$$

$$\theta_s = \tan^{-1}(W_s / 2D_s) \tag{2}$$

where θ_s is the half angle of the view, W_s is the width of the captured scope, and D_s is the distance between the injection experiments facility and the camera. During this high-speed photography, maximum error resulting from the view angle was 1.12 %, which was within the reasonable calculation error [36].

As a practical mathematical and statistical tool for efficient modeling and analyzing of process variables, this study frequently used the RSM for interactive effects between relevant parameters on the responses. In the injection experiments, the researchers used the historical data method of the RSM to observe the effect of injection parameters on the injection depth, the width of dispersion region and the percent delivery of the injection. Consequently, the mathematical model of each response can be derived by the least squares method on the basis of the following second-order polynomial regression expression (Eq. (3)):

$$\begin{aligned} Y_{(n)} = {} & B_0^{(n)} + B_1^{(n)} x_1 + B_2^{(n)} x_2 + B_3^{(n)} x_3 + \\ & B_{12}^{(n)} x_1 x_2 + B_{13}^{(n)} x_1 x_3 + B_{23}^{(n)} x_2 x_3 + \\ & B_{11}^{(n)} x_1^2 + B_{22}^{(n)} x_2^2 + B_{33}^{(n)} x_3^2 + \beta_{(n)} \end{aligned} \tag{3}$$

where B_0, B_1, B_2, B_3, B_4 and B_5 are constant; n = 1, 2, 3, 4, 5; x_1, x_2 and x_3 are factors.

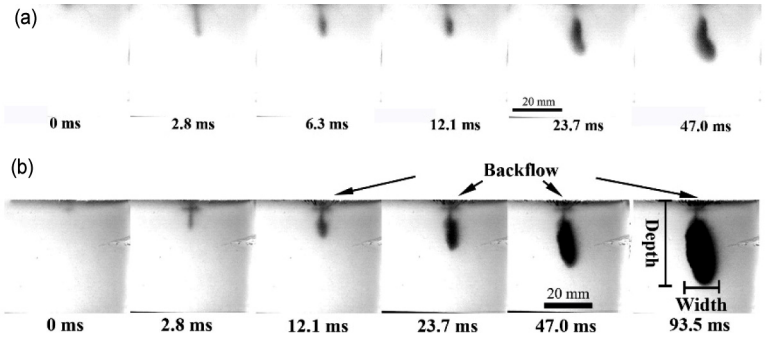

Fig. 2. Frames from high-speed video taken of the (a) 0.30 mL; (b) 1.0 mL needle-free jet injection into ballistic gelatins. The orifice diameter is 0.30 mm, the driving pressure is 0.5 MPa, and the scale bar is 20 mm long.

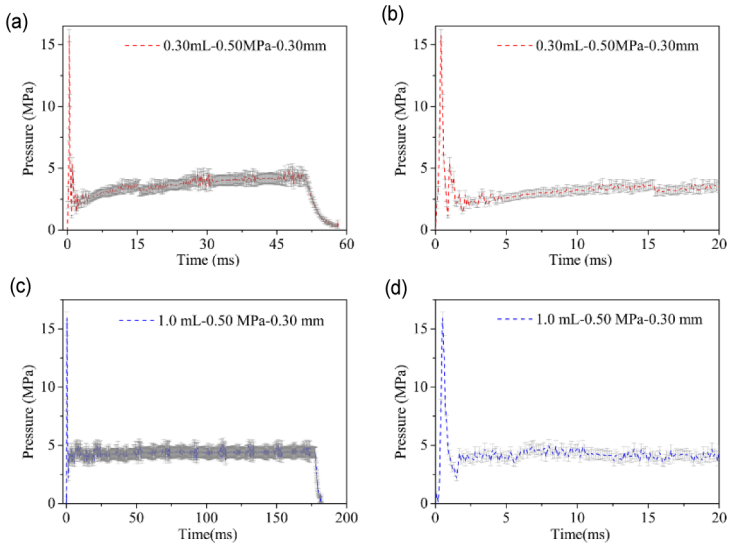

Fig. 3. Impact pressures throughout the injection process and in the first 20 ms of injection. Pressure profiles of the entire injection process with the injection volume of (a) 0.3 mL; (c) 1.0 mL; diagram of impact pressure for the injection volume of (b) 0.3 mL; (d) 1.0 mL in the first 20 ms.

The calculation of the jet power was according to our previous study [35], as shown in Eq. (4).

$$E_0 = \frac{1}{8}\pi\rho D_0^2\left[\frac{V}{A_0 T}\right]^3 = 8\rho\frac{1}{\pi^2 T^3}\frac{V^3}{D_0^4} \quad (4)$$

where E_0 is the jet power at the nozzle exit, ρ is the liquid density, V is the injection volume, T is the injection duration, and D_0 is the orifice diameter of the injector.

3. Results and discussion

3.1 Dynamics characteristics

3.1.1 Injection processes

Fig. 2 presents the dynamics of jet penetration into gels of needle-free injection process with a high-speed camera system. Fig. 2(a) exhibits the typical dispersion pattern of small volume jet injection which was an introductory channel followed by a large circular dispersion [37, 38]. For the first phase (0 ms $< t <$ 12.1 ms, where t = time after start of injection), the injection depth increased while the width of the dispersion region was the same. Then, the remaining fluid was delivered to the gels which resulted in a bolus shape in the gel (12.1 ms $< t <$ 47 ms). However, different diffusion characteristics existed in the larger volume injection (such as 1.0 mL). Fig. 2(b) shows that the injection depth and the area of the dispersion region increased during the entire injection process (0 ms $< t <$ 93.5 ms). This means that the velocity of the remaining jet arriving at the progressive end of the hole drops still exceeds the value necessary for hole formation. Interestingly, for 12.1 ms $< t <$ 47 ms, the backflow of the jet was clearly observed in gel injection when the injection volume was 1.0 mL, while this phenomenon did not occur in smaller volume injection. It was owning to that the volumetric flow rate of the 1.0 mL volume injection penetrating into the gel is greater than the volumetric rate of hole formation in the gel. Therefore, the larger volume injection is likely obtain more energy than the small volume injection in air-powered needle-free injector.

Fig. 3 displays the pressure profiles of needle-free injection

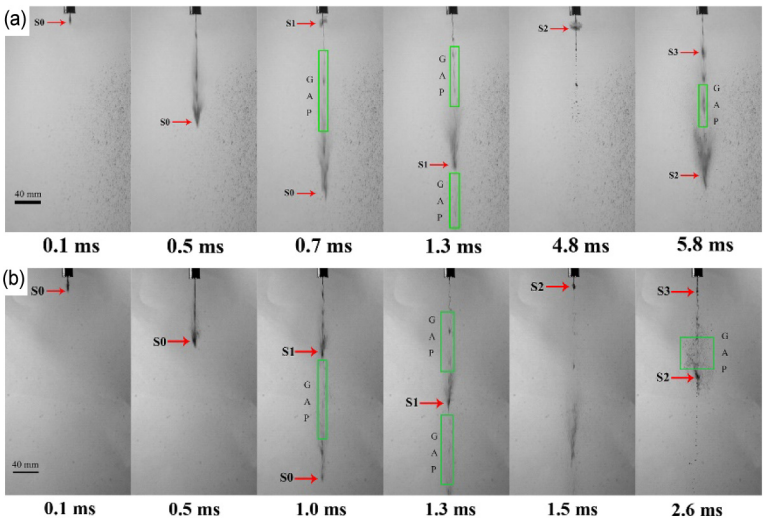

Fig. 4. Frames from a high-speed video of a water jet start-up phase for the needle-free injector with the injection volume of (a) 0.3 mL; (b) 1.0 mL. The orifice diameter is 0.30 mm, the driving pressure is 0.5 MPa, and the scale bar is 40 mm long.

with injection volumes of 0.30 mL and 1.0 mL. The injection pressure reached the maximum value shortly after the start of the injection and then dropped to a stable value. The maximum pressure value of impact experiments with injection volumes of 0.30 mL and 1.0 mL exceeded 15 MPa which is the threshold pressure at which the jet can penetrate the skin [39]. Figs. 3(a) and (b) show that the pressure tends to be stable at 5 ms after injection and the pressure variation in the stable phase fluctuates between 2.5 and 3.8 MPa. Compared with the case of injection volume of 0.30 mL, the injection pressure of 1.0 mL injection volume reached a steady phase 3 ms earlier than the former. Given the destructive force of the pulsating pressure is greater than that of the stable pressure under the same pressure value. This confirmed the phenomenon presented in the Fig. 2 shows that the injection depth at the case of 0.3 mL was greater than that at the case of 1.0 mL at the same early time point after injection. In addition, the pressure fluctuations of the 1.0 mL injection volume in the stable phase are negligible and the pressure is maintained near 4.5 MPa (see Figs. 3(c) and (d)). The difference in the steady pressure between the two would result in different injection depths and widths of the dispersion regions.

3.1.2 Early jet dynamics

To reveal the early jet dynamics of this injection, observing the behavior of the jet as it exits into the atmosphere was necessary. Fig. 4 demonstrates the start of the jet of air-powered needle-free injection with the injection volumes of 0.3 mL and 1.0 mL. The dynamic features that occurred on the microsecond to millisecond time scale of the injection were presented with the high frame rates herein. Three distinct jet pulsations of 0.3 mL volume injection were captured in Fig. 4(a), which were S1, S2, S3. The phenomena of jet pulsation are potentially related to the system compliance and compressibility when the piston is actuated by the trigger. As the liquid exits from the nozzle orifice, there is an initial jet injection (S0) and the first jet pulsation occurs at the time of 0.7 ms (S1). Likewise, the second and third jet pulsations were presented at the time of 4.8 ms and 5.8 ms. The gap between S3 and S2 is smaller than the gap between S1 and S0, which indicates that the pulsation amplitude of the jet was reduced and the steady jet will appear. In this injection case, the steady jet formation occured after 5.8 ms.

Similarly, three obvious jet pulsations exist for the dynamic features of the start-up phase of 1.0 mL volume injection (see in Fig. 4(b)). As the injection continues, the gap between the next two pulses is smaller than the gap between the two pulses at the beginning. The difference between the two injection volumes is the time to achieve stable injection. For t = 2.6 ms, S2, and S3 appear in the frame simultaneously, meaning that the steady jet formation would occur after 2.6 ms. However, for 0.3 mL injection volume, the time to achieve stable injection is 5.8 ms after start of injection. This phenomenon is consistent with the variation tendency of injection pressure in Fig. 3. Therefore, a steady jet of a larger volume injection tends to appear earlier than that of a small volume injection.

Fig. 5 displays the relationship between the axial pressure oscillation peak (P_{max}) and injection parameters in the air-powered needle-free injection. The P_{max} determines whether the jet injection can penetrate the epidermal layer of the skin. P_{max} exceeds 15 MPa in all injection conditions, so all jets can penetrate the skin. The driving pressure would lead the increase of P_{max}. Fig. 5(a) reveals this phenomenon which shows the P_{max} versus the driving pressure. Significantly, the P_{max} changes minimally and attempts to maintain a stable value when the driving pressure is greater than 1 MPa. In addition, the P_{max} of a larger volume injection is larger than that of a small volume injection, which is different from the conclusion that the maximum stagnation pressure decreases with the increasing of liquid volume in spring-loaded injector [40]. The

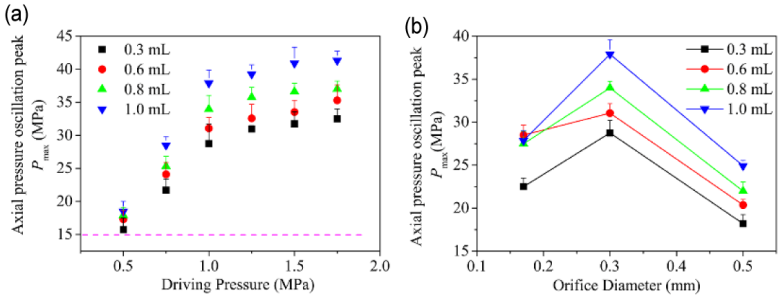

Fig. 5. (a) Relationship between the axial pressure oscillation peak and driving pressure. The orifice diameter is 0.3 mm; (b) diagram of the axial pressure oscillation peak with the change of orifice diameter. The driving pressure is 1.0 MPa.

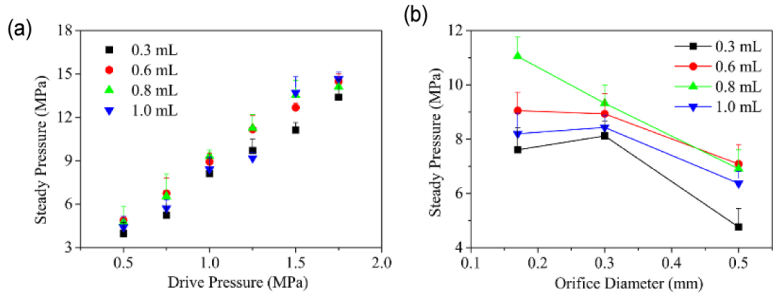

Fig. 6. The relationship between steady pressure and injection parameters. The orifice diameter in (a) is 0.3 mm; the driving pressure in (b) is 1.0 MPa.

reason is that the kinetic energy of the spring in the spring-loaded injector is constant, and the speed of the larger volume injection is smaller than that of the small volume according to the conservation of energy. However, the kinetic energy of a larger volume injection will be greater than that of a small volume injection due to the characteristics of the air-powered driving device. Fig. 5(b) plots the P_{max} versus the orifice diameter of the injector; unlike the driving pressure, a peak value of the P_{max} appears when the orifice diameter is 0.3 mm. In addition to the peak value, the P_{max} with the orifice diameter of 0.5 mm is smaller than that with the orifice diameter of 0.17 mm. Furthermore, a same tendency that a larger volume injection owns a larger value of the P_{max} is found when the orifice diameter is changed from 0.3 mm to 0.5 mm. On the contrary, no obvious change of the P_{max} transpired when the injection volume ranged from 0.6 mL-1.0 mL and the orifice diameter is 0.17 mm.

3.1.3 Steady impact pressures

The steady pressure of the jet ejected from the injector significantly influences the injection performance. Higher steady pressure leads to greater injection depth and wider injection area. To describe the effect of injection parameters on the impact pressure in the steady phase of injection, Fig. 6 demonstrates the relationship between the steady pressure and injection parameters. Fig. 6(a) illustrates that the steady pressure increases linearly as the driving pressure increases. In addition, the steady pressure between the different injection volumes did not show a significant difference at the same driving pressure. Fig. 6(b) presents the steady pressure versus the orifice diameter of the injector. When the orifice diameter is changed from 0.17 mm to 0.3 mm, the steady pressures of different injection volumes present minimal change except for the 0.8 ml injection volume. Moreover, the increasing orifice diameter decreases the steady pressure under various injection volumes when the orifice diameter is over than 0.3 mm. The difference between the steady pressures of the various injection volumes reaches a minimal value when the orifice diameter is 0.3 mm.

Similarly, the injection duration is an important parameter for evaluating injection performance [11, 12]. Studies about the influences of orifice diameter and injection volume on the injection duration has been conducted experimentally. Fig. 7(a) indicates that the increasing orifice diameter decreases injection duration, whereas increasing injection volume increases injection duration. In addition, the duration decreases sharply as the orifice diameter increases from 0.17 mm to 0.3 mm, while the duration shows a gradual decrease as the orifice diameter increases from 0.3 mm to 0.5 mm. Fig. 7(b) reveals the phenomenon that the larger volume is easier to obtain a greater proportion of stable injection time compared with the small injection volume. The proportion is more than 75 % when the injection volume exceeds 0.6 mL. The maximum values of this proportion for various injection volumes are all observed at the orifice diameter of 0.3 mm. In conjunction with the above results, there may be a suitable orifice diameter for better injection performance in the air-powered needle-free injection with various injection volumes and the orifice diameter is likely to be close to 0.3 mm.

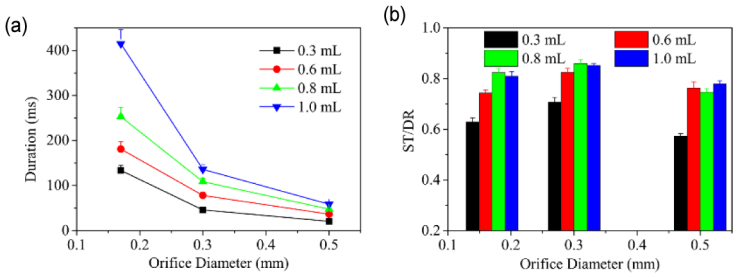

Fig. 7. (a) Curves of the injection duration versus orifice diameter of injector; (b) the relationship between the ratio of the stable period to the injection duration and orifice diameter of the injector.

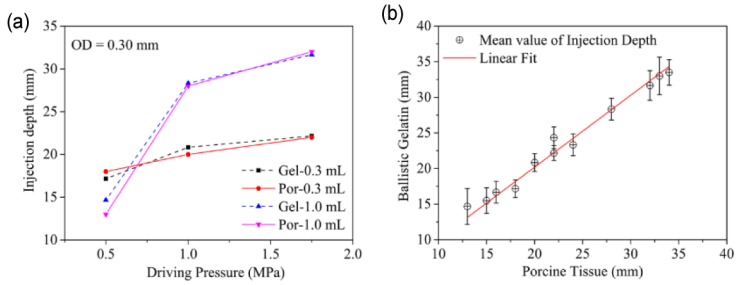

Fig. 8. (a) Variation of injection depth under different driving pressure of porcine tissues and ballistic gelatins; (b) diagram of the relationships for injection depths of porcine tissues and ballistic gelatins (y = 1.01 x).

3.2 Dispersion pattern

3.2.1 Verification of injection depth

Through the injection experiments of the gels and porcine tissues, the researchers compared the dispersion patterns of penetration characteristics of needle-free injection. Fig. 8(a) exhibits that the injection depth for the gel injections and porcine tissue injection with the injection volume of 0.3 mL and 1.0 mL increased with the increase of the driving pressure. However, the difference of the injection depth between the gel injection and porcine tissue injection is negligible under the same injection parameters. Fig. 8(b) shows a linear fit of the mean value of injection depth for the gel injections and porcine tissue injection. The ratio of the injection depth between the ballistic gelatin and porcine tissue is 1:1.01, indicating that the ballistic gelatin has similar mechanical properties to porcine tissue in the needle-free injection. Moreover, the standard error of this fit is 0.019 and the Adj. R-Square is 0.979. The differences in permeability between gelatin and porcine tissue will lead to slightly distinct injection widths. Ultimately, the ballistic gelatin is reliable as a model soft material to mimic muscular tissue in studies of needle-free injection.

3.2.2 Gels injection experiments

Fig. 9 presents the interactive effects of injection parameters, including driving pressure, orifice diameter, and injection volume, on the injection depth in the gel's injection experiments. Fig. 9(a) shows that the driving pressure and the orifice diameter of the injector positively affects the injection depth. In addition, only one fixed combination exists between the driving pressure and orifice diameter for the constant value of injection depth. For instance, when the driving pressure is 1.0 MPa, the orifice diameter must be set to 0.3 mm to reach a 25 mm injection depth.

Fig. 9(b) displays the interactive effect between the driving pressure and injection volume on the injection depth. Interestingly, the driving pressure positively affects the injection depth only when the injection volume exceeds 0.6 mL. The figure shows that the driving pressure influences the injection depth when it is lower than 1.0 MPa in the 0.3 mL volume injection; whereas no change of the injection depth is observed as the driving pressure increases from 1.0 MPa to 2.0 MPa. However, for 1.0 mL volume injection, the injection depth increases as the increasing driving pressure. Similarly, Fig. 9(c) indicates that the orifice diameter of the injector positively affects the injection depth and the increasing injection volume positively influences the injection depth as well when the injection volume is less than 0.6 mL. This phenomenon reveals a critical value exists on injection volume, which distinguishes the larger volume injection and small volume injection, meanwhile the critical value is likely to be nearly 0.6 mL.

3.2.3 Width of the dispersion region

Fig. 10 presents the interactive effects of injection parameters on the width of dispersion region. Fig. 10(a) shows that peak values of the width transpires under the interactive effect between the driving pressure and orifice diameter. The width increases with the increasing orifice diameter when the orifice diameter is less than 0.3 mm, whereas the width decreases as the orifice diameter increases when the orifice diameter ex-

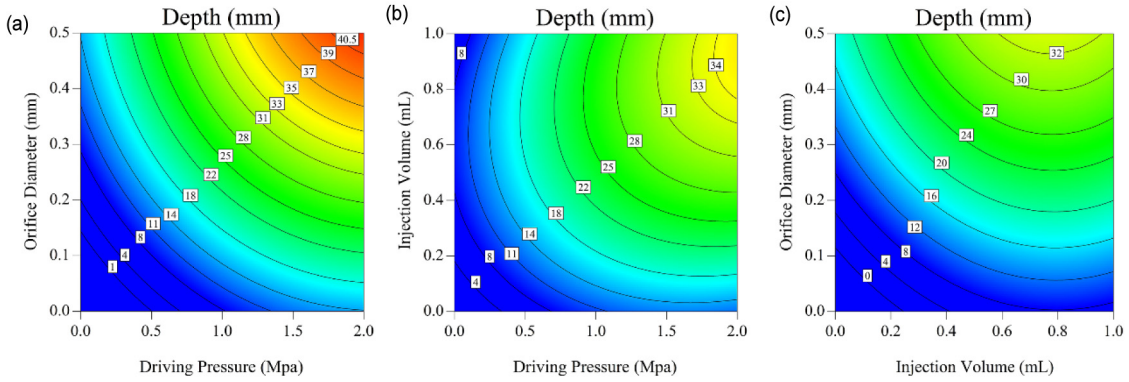

Fig. 9. Interactive effects of injection parameters on the injection depth: (a) driving pressure and orifice diameter, the injection volume is 0.6 mL; (b) driving pressure and Injection volume, the orifice is 0.3 mm; (c) injection volume and orifice diameter, the driving pressure is 1.0 MPa.

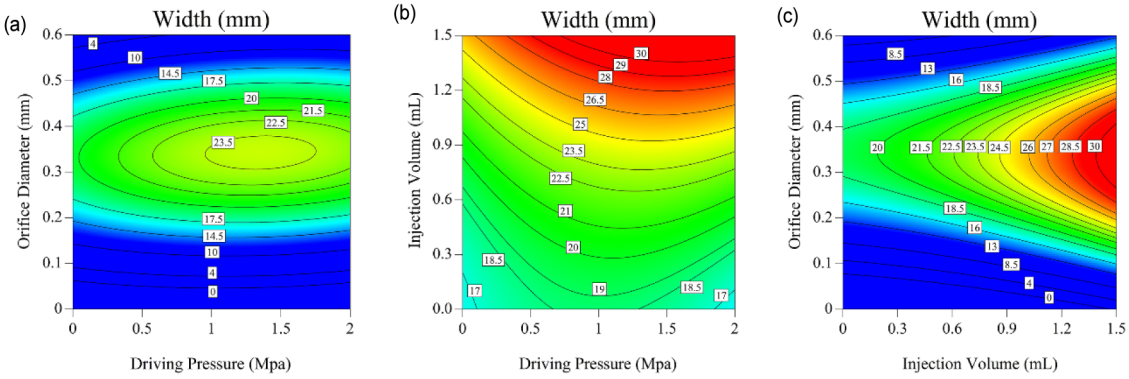

Fig. 10. Interactive effects of injection parameters on the width of dispersion region: (a) driving pressure and orifice diameter, the injection volume is 0.6 mL; (b) driving pressure and injection volume, the orifice diameter is 0.3 mm; (c) injection volume and orifice diameter, and the driving pressure is 1.0 MPa.

ceeds 0.3 mm. In addition, this study found no change of the width with the variation of the driving pressure. Similarly, the value of the width owns slight fluctuation when the driving pressure changes from 0.5 MPa to 1.5 MPa (see Fig. 10(b)). On the contrary, the increasing injection volume leads to a linear increase of the width of the dispersion region. Fig. 10(c) shows the results of the interactive effects between injection volume and orifice diameter on the width. Compared with Fig. (a), the orifice diameter of 0.3 mm plays an analogous role in the variation of the width. The maximum value of the width usually appears in this value of the orifice diameter for various injection volumes. Furthermore, the width shows an obvious increase as the injection volume increases from 0.6 mL to 1.0 mL when the orifice diameter is 0.3 mm.

3.3 Percent delivery and jet power

3.3.1 Analyses for percent delivery

The researchers explored the relationships between the percent delivery and various injection parameters in the porcine tissue injection experiments. A previous study revealed that the needle-free injection with percent delivery >90 % was considered a satisfactory injection experience [41]. Different from the effect of injection parameters on the injection depth and the width of the dispersion region, a peak value (>90 %) of the percent delivery under the interactive effects of the three injection parameters exists (see Fig. 11). Fig. 11(a) presents the correlation between the delivery percent and the interactive between the driving pressure and injection volume. The increasing driving pressure is contributed to improve the percent delivery at various injection volumes. The peak value of the percent delivery is nearly 95 % in the case where the driving pressure ranges from 1.0 MPa-1.5 MPa and the injection volume is 0.6 mL-0.9 mL. In addition, the larger volume (>0.6 mL) is more likely to acquire a higher percent delivery than the small volume injection when the driving pressure ranged from 0.5 MPa-1.5 MPa.

Similarly, Fig. 11(b) displays the interactive effect between the orifice diameter and injection volume on the percent delivery. The percent delivery exceeds 80 % when the orifice diameter is 0.3 mm-0.5 mm and the injection volume is 0.3 mL-1.2 mL. In addition, the increasing orifice diameter increases the percent delivery, whereas the variation of the injection volume does not influence the percent delivery. For the 0.3 mL-0.9 mL volume injection, a maximum value of the percent delivery (>90 %) exists when the orifice diameter is 0.3 mm-0.4 mm. Conversely, the percent delivery is often 80 % for the 0.3 mm diameter injection regardless of the change of the in-

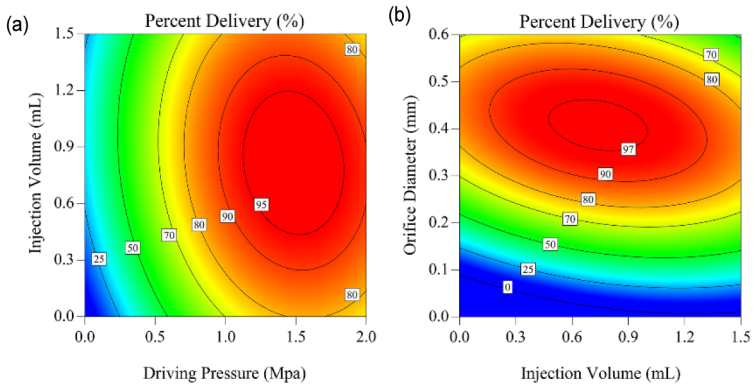

Fig. 11. Interactive effects of injection parameters on percent delivery: (a) driving pressure and injection volume, the orifice diameter is 0.3 mm; (b) injection volume and orifice diameter, and the driving pressure is 1.0 MPa.

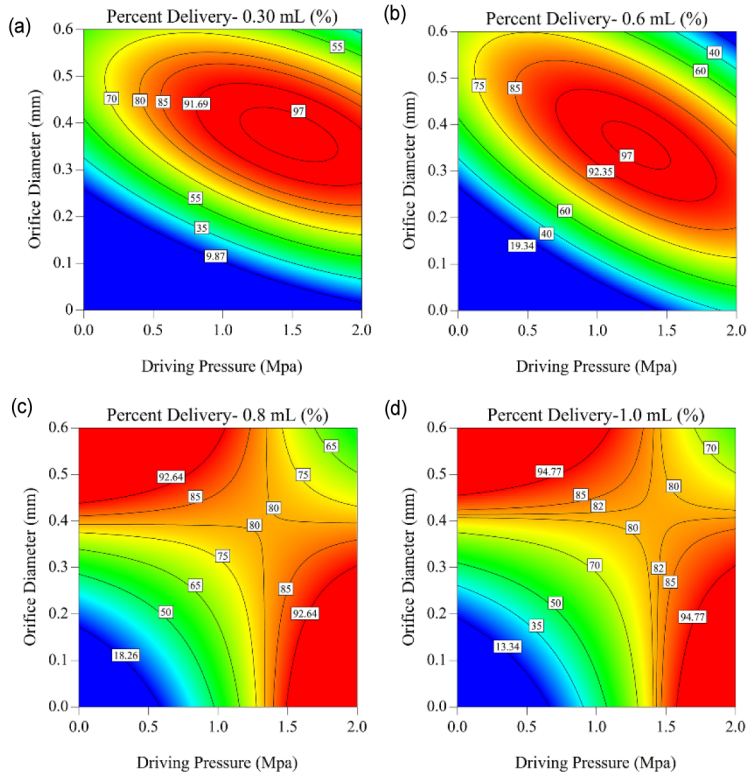

Fig. 12. Interactive effect of driving pressure and orifice diameter on percent delivery for various injection volumes: (a) 0.3 mL; (b) 0.6 mL; (c) 0.8 mL; (d) 1.0 mL.

jection volume.

The interactive effect between driving pressure and orifice diameter plays the most important role in the performance of percent delivery. Various combinations of the orifice diameter and driving pressure will help the percent delivery to obtain higher values for various injection volumes (Fig. 12). Regarding the 0.3 mL volume injection in Fig. 12(a), the increasing orifice diameter can increase the percent delivery. The percent delivery for the injections with orifice diameters of 0.3 mm-0.5 mm exceeds 80 % when the driving pressure is 1.0 MPa-1.5 MPa. The percent delivery of injections with different orifice diameters reaches the maximum value when the driving pressure is approximately 1.5 MPa. Fig. 12(b) reveals that the percent delivery exceeds 90 % in the case where the orifice diameter is 0.3 mm and the driving pressure is more than 1.0 MPa. The peak value of the percent delivery appears in the range of 1.0 MPa to 1.5 MPa when the orifice diameter is 0.3 mm for the 0.6 mL volume injection.

A significant difference is present between the larger volume injection (0.8 mL and 1.0 mL) and small volume injection (0.3 mL and 0.6 mL) in the variation of the percent delivery. Figs. 12(c) and (d) exhibit that the increasing driving pressure

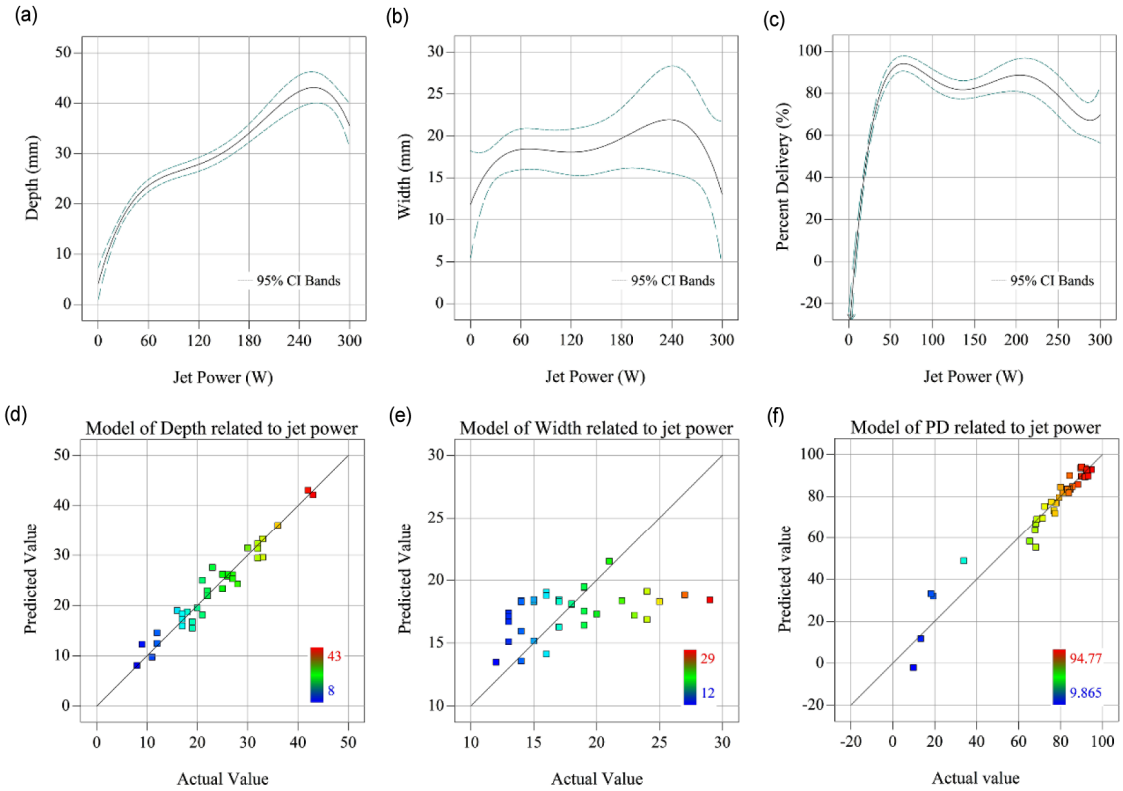

Fig. 13. The RSM analysis results related to jet power: (a) the curve of the injection depth versus jet power; (b) the curve of the width of the dispersion region versus jet power; (c) the curve of the percent delivery versus jet power; (d) scatter plot of predicted and actual values for the model of injection depth related to jet power; (e) scatter plot of predicted and actual values for the model of the dispersion region related to jet powers; (f) scatter plot of predicted and actual values for the model of the percent delivery related to jet powers (PD represents the delivery percent). The driving pressure is maintained at 1.0 MPa, the injection volume ranges from 0 to 1.0 mL and the nozzle diameter ranges from 0.17-0.50 mm.

increases the value of the percent delivery when the orifice diameter is less than 0.3 mm. On the contrary, the percent delivery decreases with the increase of the driving pressure in the case where the orifice diameter exceeds 0.3 mm. The peak values of the percent delivery with orifice diameters of 0.1 mm-0.3 mm usually occur at a small driving pressure, while that with orifice diameters of 0.4 mm to 0.6 mm appear when the driving pressure is nearly 1.5 MPa. The former result differs greatly from the small volume injections, whereas the latter phenomenon is consistent with the small volume injections in Figs. 12(a) and (b).

3.3.2 Analyses for jet power

The jet power at the exit of the nozzle is often considered a composite indicator for injection parameters in the needle-free injection. Then we conduct studies on the effect of jet power on the injection depth, the width of the dispersion, and the percentage of the liquid delivered to porcine tissues. Fig. 13(a) shows the relationship between the jet power and injection depth. The injection depth increases as the jet power when the jet power is less than 240 W. A sharp increase transpires for the injection depth in the case where the jet power is 0-60 W. As the jet power continues to increase to 240 W, the injection depth slowly increases. Interestingly, the injection depth tends to decrease when the jet exceeds 240 W. Based on the experimental data, the regression model for injection depth related to jet power is shown in Eq. (5). Fig. 13(d) displays the scatter plot of predicted and actual values for the model of injection depth related to jet power. The *Adj R-squared* of this model is 0.9589 and the *Pred R-squared* of this model is 0.9529, implying that this model is reliable to predicate the behavior of the injection depth related to jet power.

$$\mathrm{Ln}(\mathrm{Depth}(Y_{(j)})) = 3.40 + 0.76x_j + 0.79x_j^{\,2} - 1.22x_j^{\,3} - 1.51x_j^{\,4} + 1.37x_j^{\,5} \quad (5)$$

where *Depth*($Y_{(j)}$) represents injection depth, and x_j represents the jet power.

Fig. 13(b) shows the curve of the jet power versus the width of the dispersion region. The figure reveals that no significant change of the width is observed when the jet power is changed from 60 W to 240 W. In addition, the model for the width associated with jet power is not suitable for predicating the relationships between the two (Fig. 13(e)). No evidence of a relationship between the jet power and the width of the dispersion region exists. Fig. 13(c) presents the relationship between the jet power and percent delivery. The percent delivery increases

sharply to 90 % when the jet power is close to 50 W which is in line with the previous research [40]. Then, the percent delivery fluctuates between 70 % and 95 % as the injection power continues to increase. To reveal the influence of the jet power on the percent delivery, this study obtained the model for the percent delivery related to the jet power using the RSM in Eq. (6). The *Adj R-squared* of this fifth model is 0.9512 and the *Pred R-squared* of this model is 0.9382 which means that this model can predict the percent delivery associated to jet power.

$$\sqrt{\mathrm{PD}(Y_{(j)})} = 9.041 + 2.257x_j + 4.407x_j^2 - 12.656x_j^3 - 8.116\times10^{-6}x_j^4 + 13.516x_j^5 \quad (6)$$

where $PD(Y_{(j)})$ represents percent delivery, x_j represents the jet power (E_0).

4. Conclusions

This study analyzed the jet dynamic characteristics and penetrations characteristics of larger volume needle-free injection device through high-speed videography and RSM. The researchers presented the various characteristics of this device with various injection volumes through impact experiments and injection experiments. On the basis of the experimental data, this study provided detailed analyses of the difference of these characteristics between the larger and the small volume injections. These results can be used to guide the development of the larger volume needle-free injection devices for better injection efficiency and a satisfactory injection experience. Hence, the following conclusions can be obtained:

(1) A critical value on injection volume exists which distinguishes the larger volume injection and small volume injection and the critical value is likely to be nearly 0.6 mL.

(2) The injection pressure of larger volume injection reaches the steady phase sooner than the small volume injection and the larger volume injection is likely obtaining more energy than the small volume injection in needle-free injection. In addition, the steady jet of a larger volume injection tends to appear earlier than that of a small volume injection.

(3) There exist optimal combinations between the orifice diameter and driving pressure for better injection performance in the needle-free injection with larger volumes injection. These combinations of the two are that the orifice diameter is nearly 0.3 mm and the driving pressure is 1.0 MPa-1.5 MPa.

(4) The jet power plays a significant role in the injection depth and percent delivery in the needle-free injection. The models for the injection depth and percent delivery associated to jet power are reliable to predicate the behavior of the penetration characteristics.

Conflicts of interest

The authors declare no financial or non-financial interests that represent potential conflict of interests.

Acknowledgements

This work was supported by the National Key R&D Program of China [grant number: 2018YFC0808401]; the National Key Basic Research Program of China [grant number: 2014CB 239203]; the National Natural Science Foundation of China (NSFC) [grant number: 51474158].

Nomenclature

θ_s : Half angle of the view
W_s : Width of the captured scope
D_s : Distance between the injection experiments facility and the camera
P_{max} : Axial pressure oscillation peak
PD : Percent delivery
RSM : Response surface methodology
E_0 : Jet power at the nozzle exit
P : Liquid density
V : Injection volume
T : Injection duration
D_0 : Orifice diameter

References

[1] S. Mitragotri, Immunization without needles, *Nature Reviews Immunology*, 5 (12) (2005) 905-916.

[2] M. R. Prausnitz, S. Mitragotri and R. Langer, Current status and future potential of transdermal drug delivery, *Nature Reviews Drug Discovery*, 3 (2) (2004) 115-124.

[3] J. O. Marston and C. M. R. Lacerda, Characterization of jet injection efficiency with mouse cadavers, *Journal of Controlled Release*, 305 (2019) 101-109.

[4] S. Mitragotri, Current status and prospects of needle-free liquid jet injectors, *Nature Reviews Drug Discovery*, 5 (7) (2006) 543-548.

[5] A. Mohizin and J. K. Kim, Current engineering and clinical aspects of needle-free injectors: A review, *Journal of Mechanical Science and Technology*, 32 (12) (2018) 5737-5747.

[6] M. A. Trimzi, Y.-B. Ham, B.-C. An, J.-H. Park and S.-N. Yun, Numerical analysis and simulation of an impulse driven piezoelectric needle-free jet injector, *Journal of Mechanical Science and Technology*, 33 (8) (2019) 3851-3858.

[7] D. Barolet and A. Benohanian, Current trends in needle-free jet injection: an update, *Clinical Cosmetic and Investigational Dermatology*, 11 (2018) 231-238.

[8] A. Bavdekar et al., Immunogenicity and safety of measles-mumps-rubella vaccine delivered by disposable-syringe jet injector in India: A randomized, parallel group, non-inferiority trial, *Vaccine*, 36 (9) (2018) 1220-1226.

[9] A. Taberner, N. C.Hogan and I. W. Hunter, Needle-free jet injection using real-time controlled linear Lorentz-force actuators, *Medical Engineering & Physics*, 34 (9) (2012) 1228-1235.

[10] A. J. Taberner, N. B. Ball, N. C. Hogan and I. W. Hunter, A portable needle-free jet injector based on a custom high

power-density voice-coil actuator, *28th Annual International Conference of the IEEE Engineering in Medicine and Biology Society*, 1-15 (2006) 2531-2534.

[11] J. C. Stachowiak, M. G. von Muhlen, T. H. Li, L. Jalilian, S. H. Parekh and D. A. Fletcher, Piezoelectric control of needle-free transdermal drug delivery, *Journal of Controlled Release*, 124 (1-2) (2007) 88-97.

[12] J. C. Stachowiak, T. H. Li, A. Arora, S. Mitragotri and D. A. Fletcher, Dynamic control of needle-free jet injection, *Journal of Controlled Release*, 135 (2) (2009) 04-12.

[13] C. B. Rodríguez, C. W. Visser, S. Schlautmann, D. F. Rivas and R. Ramos-García, Toward jet injection by continuous-wave laser cavitation, *Journal of Biomedical Optics*, 22 (10) (2017) 9.

[14] N. C. Hogan, A. J. Taberner, L. A. Jones and I. W. Hunter, Needle-free delivery of macromolecules through the skin using controllable jet injectors, *Expert Opinion on Drug Delivery*, 12 (10) (2015) 1637-1648.

[15] P. Rohilla and J. O. Marston, In-vitro studies of jet injections, *International Journal of Pharmaceutics*, 568 (2019) 118503.

[16] J. E. Epstein, E. Y. Gorak, R. Wang, N. Freydberg, O. Osinowo and T. L. Richie, Safety, tolerability, and lack of antibody responses after administration of a PfCSP DNA malaria vaccine via needle or needle-free jet injection, and comparison of intramuscular and combination intramuscular/intradermal routes, *Human Gene Therapy*, 13 (13) (2002) 1551-1560.

[17] L. H. Nicoll and A. Hesby, Intramuscular injection: An integrative research review and guideline for evidence-based practice, *Applied Nursing Research*, 15 (3) (2002) 149-162.

[18] N. Kojic, P. Goyal, C. H. Lou and M. J. Corwin, An innovative needle-free injection system: Comparison to 1 ml standard subcutaneous injection, *AAPS Pharm Sci. Tech.*, 18 (8) (2017) 2965-2970.

[19] B. P. Ruddy, J. W. McKeage, R. M. J. Williams, P. M. F. Nielsen and A. J. Taberner, A compound ampoule for large-volume controllable jet injection, *IEEE Engineering in Medicine and Biology Society Annual Conference*, 2015 (2015) 7341-7344.

[20] J. W. McKeage, B. P. Ruddy, P. M. F. Nielsen and A. J. Taberner, The effect of jet speed on large volume jet injection, *Journal of Controlled Release*, 280 (2018) 51-57.

[21] J. W. McKeage, B. P. Ruddy, P. M. F. Nielsen and A. J. Taberner, Power-efficient controlled jet injection using a compound ampoule, *Journal of Controlled Release*, 291 (2018) 127-134.

[22] D. Zeng, N. Wu, L. Qian, H. Shi and Y. Kang, A novel controllable pneumatic needle-free injection system for larger-volume drug delivery, *Journal of Pharmaceutical Sciences*, 109 (5) (2020) 1772-1779.

[23] R. Portaro and H. D. Ng, Experiments and modeling of air-powered needle-free liquid injectors, *Journal of Medical and Biological Engineering*, 35 (5) (2015) 685-695.

[24] T. M. Grant, K. D. Stockwell, J. B. Morrison and D. D. Mann, Effect of injection pressure and fluid volume and density on the jet dispersion pattern of needle-free injection devices, *Biosystems Engineering*, 138 (2015) 59-64.

[25] P. Rohilla, Y. S. Rane, I. Lawes, A. Le Blanc, J. Davis and J. B. Thomas, Characterization of jets for impulsively-started needle-free jet injectors: Influence of fluid properties, *Journal of Drug Delivery Science and Technology*, 53 (2019) 101167.

[26] H. Nakayama, R. Portaro, C. B. Kiyanda and H. D. Ng, CFD modeling of high speed liquid jets from an air-powered needle-free injection system, *Journal of Mechanics in Medicine and Biology*, 16 (4) (2016) 1650045.

[27] R. Zahoor, S. Bajt and B. Šarler, Influence of gas dynamic virtual nozzle geometry on micro-jet characteristics, *International Journal of Multiphase Flow*, 104 (2018) 152-165.

[28] J. Seok, C. T. Oh, H. J. Kwon, T. R. Kwon, E. J. Choi and S. Y. Choi, Investigating skin penetration depth and shape following needle-free injection at different pressures: A cadaveric study, *Lasers in Surgery & Medicine*, 48 (6) (2016) 624-628.

[29] R. Williams, J. W. McKeage, B. P. Ruddy, P. F. Nielsen and A. Taberner, Viscous heating assists jet formation during needle-free jet injection of viscous drugs, *IEEE Transactions on Biomedical Engineering* (2019) 1.

[30] J. A. Simmons, J. Davis, J. Thomas, J. Lopez, A. Le Blanc and H. Allison, Characterization of skin blebs from intradermal jet injection: Ex-vivo studies, *Journal of Controlled Release*, 307 (2019) 200-210.

[31] A. Mohizin, K. E. R. Roy, D. Lee, S. K. Lee and J. K. Kim, Computational fluid dynamics of impinging microjet for a needle-free skin scar treatment system, *Computers in Biology and Medicine*, 101 (2018) 61-69.

[32] J. Jussila, Preparing ballistic gelatine—review and proposal for a standard method, *Forensic Science International*, 141 (2) (2004) 91-98.

[33] K. Comley and N. Fleck, Deep penetration and liquid injection into adipose tissue, *Journal of Mechanics of Materials and Structures*, 6 (1-4) (2011) 127-140.

[34] D. Zeng, Y. Kang, L. Xie, X. Xia, Z. Wang and W. Liu, A mathematical model and experimental verification of optimal nozzle diameter in needle-free Injection, *Journal of Pharmaceutical Sciences,* 107 (4) (2018) 1086-1094.

[35] D. Zeng, N. Wu, L. Xie, X. Xia and Y. Kang, An experimental study of a spring-loaded needle-free injector: Influence of the ejection volume and injector orifice diameter, *Journal of Mechanical Science and Technology,* 33 (11) (2019) 5581-5588.

[36] A. M. Abdulaziz, Performance and image analysis of a cavitating process in a small type venture, *Experimental Thermal & Fluid Science*, 53 (2) (2014) 40-48.

[37] J. Schramm-Baxter, J. Katrencik and S. Mitragotri, Jet injection into polyacrylamide gels: Investigation of jet injection mechanics, *Journal of Biomechanics,* 37 (8) (2004) 1181-1188.

[38] B. D. Hemond, A. Taberner, C. Hogan, B. Crane and I. W. Hunter, Development and performance of a controllable autoloading needle-free jet injector, *Journal of Medical Devices-Transactions of the ASME,* 5 (1) (2011).

[39] O. A. Shergold, N. A. Fleck and T. S. King, The penetration of a soft solid by a liquid jet, with application to the administration of a needle-free injection, *Journal of Biomechanics*, 39 (14) (2006) 2593-2602.

[40] K. Chen and H. Zhou, An experimental study and model validation of pressure in liquid needle-free injection, *International Journal of Physical Sciences* (2011).
[41] J. Schramm-Baxter and S. Mitragotri, Needle-free jet injections: dependence of jet penetration and dispersion in the skin on jet power, *Journal of Controlled Release*, 97 (3) (2004) 527-535.

Dongping Zeng received his B.S. degree from Northwest Agriculture Forestry University, Xian, China, in 2016, and is now a Ph.D. candidate in School of Power and Mechanical Engineering, Wuhan University, Wuhan, China. He focuses on the mechanical principle and clinic application of needle-free jet injector.

Yong Kang received his B.S. and Ph.D. degrees from Chongqing University, China, in 2001 and 2006. He is now a Professor and the vice dean of the School of Mechanical Engineering, Wuhan University, Wuhan, China. His research interests include biomedical engineering, water-jet technology, and mining technology.